materials

MDPI

Article

Magnetic $CuFe_2O_4$ Spinel–Polypyrrole Pseudocapacitive Composites for Energy Storage

Mahmoud Awad and Igor Zhitomirsky *

Department of Materials Science and Engineering, McMaster University, Hamilton, ON L8S 4L7, Canada; awadm11@mcmaster.ca

* Correspondence: zhitom@mcmaster.ca

Abstract: This investigation focused on the fabrication of ceramic ferrimagnetic $CuFe_2O_4$–conductive polypyrrole (PPy) composites for energy storage. $CuFe_2O_4$ with a crystal size of 20–30 nm and saturation magnetization of 31.4 emu g^{-1} was prepared by hydrothermal synthesis, and PPy was prepared by chemical polymerization. High-active-mass composite electrodes were fabricated for energy storage in supercapacitors for operation in a sodium sulfate electrolyte. The addition of PPy to $CuFe_2O_4$ resulted in a decrease in charge transfer resistance and an increase in capacitance in the range from 1.20 F cm^{-2} (31 F g^{-1}) to 4.52 F cm^{-2} (117.4 F g^{-1}) at a 1 mV s^{-1} sweep rate and from 1.17 F cm^{-2} (29.9 F g^{-1}) to 4.60 F cm^{-2} (120.1 F g^{-1}) at a 3 mA cm^{-2} current density. The composites showed higher capacitance than other magnetic ceramic composites of the same mass containing PPy in the same potential range and exhibited improved cyclic stability. The magnetic behavior of the composites was influenced by the magnetic properties of ferrimagnetic $CuFe_2O_4$ and paramagnetic PPy. The composites showed a valuable combination of capacitive and magnetic properties and enriched materials science of magnetic supercapacitors for novel applications based on magnetoelectric and magnetocapacitive properties.

Keywords: spinel; copper ferrite; polypyrrole; composite; supercapacitor; hydrothermal synthesis; ferrimagnetism

check for updates

Citation: Awad, M.; Zhitomirsky, I. Magnetic $CuFe_2O_4$ Spinel–Polypyrrole Pseudocapacitive Composites for Energy Storage. *Materials* **2024**, *17*, 5249. https://doi.org/10.3390/ma17215249

Academic Editor: Antonio Caggiano

Received: 2 October 2024
Revised: 23 October 2024
Accepted: 26 October 2024
Published: 28 October 2024

Copyright: © 2024 by the authors. Licensee MDPI, Basel, Switzerland. This article is an open access article distributed under the terms and conditions of the Creative Commons Attribution (CC BY) license (https://creativecommons.org/licenses/by/4.0/).

1. Introduction

Ceramic–conductive polymer composites have attracted rising attention due to their advanced multifunctional properties and interesting interface effects, which result in enhanced magnetoresistance, conductivity, magnetization, charge storage, and other properties [1–4]. Moreover, the addition of conductive polymers to ceramics improves the processability of ceramic–polymer nanocomposites [4]. Conductive polymers show valuable capacitive properties for energy storage applications [5–10]. (LaSr)MnO_3 (LSMO)–polyaniline (PANI) composites showed enhanced conductivity and magnetoresistance in [1]. It was demonstrated that the synergistic effects in the composites resulted from the influence of the PANI coating on the LSMO particles on the electric transport and magnetoelectric phenomena in the magnetic fields. A magnetoresistance increase of ~73% was reported in the composites containing LSMO particles coated with PANI [11]. Polypyrrole (PPy) coatings on LSMO particles were developed in [3], and such coatings influenced the charge transfer, double-exchange interactions, and magnetization. Of particular interest was the significant enhancement in magnetization from 49.4 to 102.0 emu g^{-1} of the core–shell particles due to the decreased spin disorder in the LSMO core [3]. The magnetization increase resulted from the transfer of charge and spin from the conductive polymer layer to the LSMO. An enhancement of saturation magnetization was also reported for PPy-coated Fe_3O_4 particles and attributed to charge transfer, which increased the surface magnetic moment of the particles [12]. An investigation of the charge storage properties of LSMO-PPy composites showed a considerable increase in electrochemical capacitance compared with

pure PPy [13]. Magnetoelectric composites have been developed for diverse applications in solar cells, memory devices, and sensors [4]. $CoFe_2O_4$-PPy composites showed advanced microwave absorption properties in [14]. ZnO-PEDOT composites exhibited promising properties for applications in electrochromic displays in [15].

Efficient CuO-PPy anodes were developed for energy storage in lithium-ion batteries in [16–19]. The composites offered the advantages of increased conductivity and capacity. Moreover, the detrimental volume changes related to charging and discharging were reduced. CuO-PPy composites showed promising performance for applications in supercapacitors with enhanced capacitance [20–22]. The investigations in [23] revealed a synergy of the charge storage properties of CuO and PPy, which led to the high capacitance of the composites. Hexagonal ferrite [24] and spinel [25] ferrimagnetic ceramics were combined with PPy for the fabrication of advanced supercapacitor composite anodes. In addition to high capacitance, such composites exhibited valuable magnetic properties.

The progress achieved in the development of ceramic–conductive polymer composites indicates that further advances in this area can result in the development of novel advanced composites containing various functional ceramic materials. Composites exhibit valuable functional properties, such as advanced mechanical properties, photovoltaic properties, high conductivity, and advanced mechanical and electrical properties, which have been utilized for novel applications [26–32]. $CuFe_2O_4$ is a promising multifunctional material for the development of ceramic–polymer composites. $CuFe_2O_4$ is a spinel ferrimagnetic compound [33,34] that exhibits high magnetization due to superexchange interactions between Cu^{2+} and Fe^{3+} ions. It is an advanced material for biomedicine [35], catalytic applications [36], water purification [37], photovoltaic [38] devices, and energy storage applications in supercapacitors [39–43]. Therefore, the development of $CuFe_2O_4$–conductive polymer composites can result in materials with advanced functionality.

This investigation was motivated by the interesting multifunctional properties of ceramic–PPy composites. Moreover, the research motivation was fueled by the multifunctional properties of $CuFe_2O_4$ and recent advances in the development of multifunctional materials [44], combining high magnetization and remarkable pseudocapacitive properties. Such materials show novel magnetoelectric effects, which are currently under consideration for the fabrication of novel multifunctional devices. Of particular interest are the results regarding capacitance increases and charge transfer resistance decreases in a magnetic field, electric potential-controlled magnetization reversal, electric potential-controlled shift of the Curie point, periodic variations in magnetization by periodic galvanostatic charge–discharge, electric field control of saturation magnetization, and other magnetocapacitive and magnetoelectric effects [44]. Different mechanisms that provide a direct link between magnetization and redox reactions were described in [44]. As pointed out above, the combination of pseudocapacitive conductive polymers and ceramic magnetic particles generates new effects related to spin transfer from the paramagnetic polymers to the magnetically ordered ceramic materials, which results in enhanced magnetization.

The objective of this work was the fabrication and testing of new $CuFe_2O_4$-PPy composites. In contrast with other studies on magnetic complex oxide ceramic–PPy composites [24,25], which involved high-energy ball milling for the particle size reduction of the ceramic phase, the fabrication of $CuFe_2O_4$ nanoparticles was performed by hydrothermal synthesis. The composite materials combined high magnetic and pseudocapacitive properties due to the synergy of the contributions of $CuFe_2O_4$ and PPy. It was found that the magnetic properties of the composites were influenced by the weakly paramagnetic PPy. The combination of $CuFe_2O_4$ and PPy resulted in improved capacitance and cyclic stability.

2. Materials and Methods

Iron (III) chloride hexahydrate ($FeCl_3 \cdot 6H_2O$), copper (II) chloride dihydrate ($CuCl_2 \cdot 2H_2O$), trisodium citrate dihydrate ($C_6H_9Na_3O_9$) (TSCD), NaOH, polyvinyl butyral (PVB), pyrrole (Py), ammonium persulfate (APS), and 4,5-dihydroxy-1,3-benzenedisulfonic acid disodium salt monohydrate (Tiron) were supplied by Aldrich. Multiwalled carbon

nanotubes (MWCNTs) (with outer and inner diameters of 12 and 5 nm, respectively, and an average length of 1.5 μm) were provided by Bayer, Germany. Ni foams (with a thickness of 1.5 mm and 95% porosity) were supplied by Vale, Ontario, Canada.

$CuFe_2O_4$ (CFO) and PPy were used for the fabrication of composite materials. CFO was selected due to its high magnetization and promising pseudocapacitive properties. PPy is an advanced pseudocapacitive material that offers the benefit of high conductivity.

The synthesis of CFO nanoparticles was performed with 7 mM of $FeCl_3$ and 3.3 mM of $CuCl_2$ as precursors. Both were dissolved in 50 mL of DI water. Then, TSCD was added as a chelating agent to the solution at 15% according to the weight of the precursors. The solution was stirred until completely dissolved. An aqueous solution of NaOH was used to adjust the pH to 12. The hydrothermal process was conducted for 8 h at 180 °C. The product was washed with DI water and ethanol several times to remove the unwanted by-products and dried for 12h at 55 °C.

The synthesis of PPy was achieved with a 0.1 M Py reagent added to DI water cooled with an ice bath to 4 °C. Tiron was added as a dopant to the solution with a Py:Tiron molar ratio of 10:1. Then, 0.1 M APS was added dropwise as an oxidizing agent. The mixture was kept under stirring for 2 h to complete the chemical reaction. Subsequently, the Tiron-doped PPy was washed with DI water to remove excess materials and dried until a constant mass was reached.

The synthesis methods used in this investigation facilitated the fabrication of stable slurries of PPyand CFO. The sedimentation tests showed the good colloidal stability of the slurries in ethanol, which facilitated improved the mixing of the individual components. Moreover, the use of Tiron as a dopant for PPy was beneficial for the improved mixing of PPy and CFO. It is known that catecholate-type materials, such as Tiron, provide strong chelating bonding to metal atoms on the surface of inorganic nanoparticles [45]. The slurries in ethanol for the impregnation of Ni foam current collectors contained the materials in a ratio of (CFO + PPY):MWCNT:PVB = 80:20:3. CFO100 samples were prepared without PPy as a control sample. Different composite materials were prepared by variations in the PPy and CFO contents in their composition to analyze the influence of the electrode composition on their properties. The preparation of electrodes with the same active mass loading and same thickness was important for the comparison of their properties. However, the limitations of this preparation method resulted from the low density of PPy. As a result, the maximum content of the PPy phase in the electrodes of the same mass and thickness was 70%. The samples CFO90, CFO70, CFO50, and CFO30 contained CFO and PPy. The CFO:PPy mass ratios were 90:10, 70:30, 50:50, and 30:70 for CFO90, CFO70, CFO50, and CFO30, respectively. The mass of the impregnated materials after drying was 40 mg cm^{-2}. To increase physical contact, the impregnated foams were pressed to 37% of their original thickness. All electrodes had an area of 1 cm^2.

Transmission Electron Microscopy (TEM) analysis was conducted using a Talos L120C system, while X-ray diffraction (XRD) patterns were recorded with a Bruker D8 Advance diffractometer (Cu-Kα radiation). Scanning Electron Microscopy (SEM) imaging was carried out with a JSM 6610LV (JEOL, Tokyo, Japan). Electrochemical investigations, including cyclic voltammetry (CV), electrochemical impedance spectroscopy (EIS), and galvanostatic charge–discharge (GCD) studies, were performed using a VMP 300 potentiostat (BioLogic, Seyssinet-Pariset, France). The magnetic data were obtained with MPMS SQUID magnetometer (Quantum Design, San Diego, CA, USA). The simulations of the EIS data were performed using the ZSimpWin software v3.6 (AMETEK, Oak Ridge, TN, USA). All electrochemical tests of the electrodes were conducted in a three-electrode setup using a 0.5 M Na_2SO_4 aqueous electrolyte. A saturated calomel electrode (SCE) served as the reference electrode, while a platinum gauze was used as the counter electrode. Equations (1) and

(2) were used to calculate the integral capacitances (C_S and C_m) by normalizing the total capacitance (C) by the electrode area and mass, respectively [46]:

$$C = \frac{\Delta Q}{\Delta U} = \frac{\left|\int_0^{t(U_{max})} Idt\right| + \left|\int_{t(U_{max})}^0 Idt\right|}{2U_{max}} \quad (1)$$

where I is the current, ΔQ is the charge, and ΔU is the potential range, and from the chronopotentiometry data:

$$C = I\Delta t/\Delta U \quad (2)$$

The complex capacitance $C^*(\omega) = C'(\omega) - iC''(\omega)$ was derived from the EIS data at various frequencies (ω) of complex impedance, where $Z^*(\omega) = Z'(\omega) + i\,Z''(\omega)$ [47]:

$$C'(\omega) = \frac{-Z''(\omega)}{\omega|Z(\omega)|^2} \quad (3)$$

$$C''(\omega) = \frac{Z'(\omega)}{\omega|Z(\omega)|^2} \quad (4)$$

3. Results and Discussion

The XRD diffraction pattern of the as-prepared material (Figure 1A) confirmed the formation of a pure spinel phase of $CuFe_2O_4$. The diffraction angles and peak intensities corresponded to JCPDS file 00-034-0425. The relatively wide peaks indicated a small particle size. The magnetic measurements (Figure 1B) showed a saturation magnetization of 31.4 emu g^{-1}, which was higher than the saturation magnetization of $CuFe_2O_4$ prepared by some other methods [48,49]. It is known that the magnetization of $CuFe_2O_4$ depends on the occupancy of the tetrahedral and octahedral positions of the spinel crystallographic unit cells by the Cu^{2+} and Fe^{3+} ions. The literature data for this material show that saturation magnetization can be in the range of 1–2.3 μ_B per molecule [34]. The saturation magnetization of magnetic materials usually decreases with decreasing nanoparticle size [50]. The analysis of magnetization versus magnetic field dependence in low fields (Figure 1B, inset) did not show hysteresis. The zero net magnetic moment in the absence of a magnetic field indicated a superparamagnetic behavior, which can result from a small crystal size.

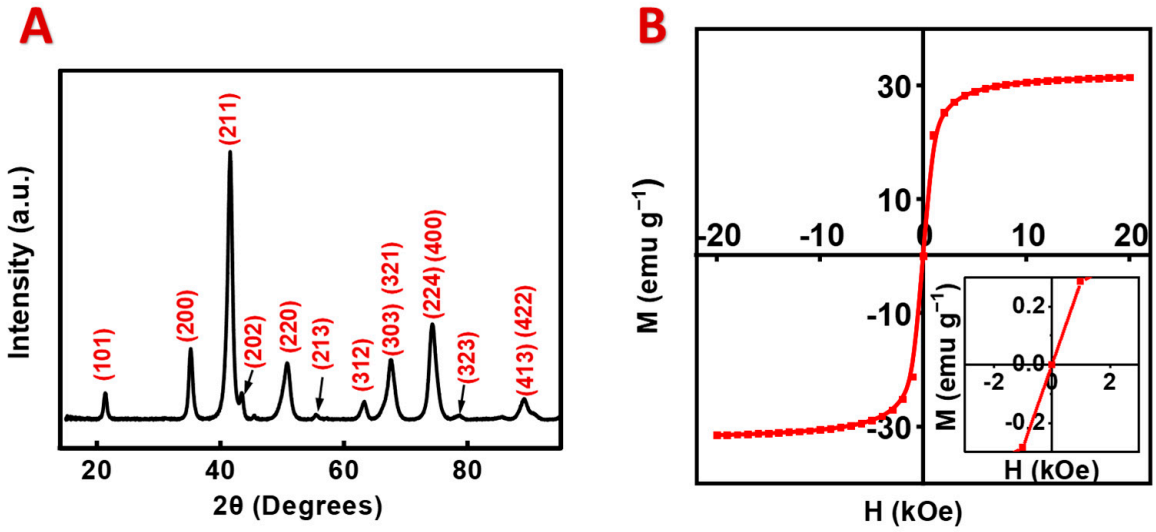


Figure 1. (**A**) X-ray X-ray diffraction pattern of $CuFe_2O_4$, prepared by hydrothermal synthesis. Miller indices of planes correspond to JCPDS file 00-034-0425. (**B**) Magnetization (M) plotted against magnetic field (H) for $CuFe_2O_4$ (inset shows low-field range).

The TEM studies (Figure 2) showed that the hydrothermal synthesis resulted in the formation of $CuFe_2O_4$ nanoparticles with a size of 20–30 nm. The TEM images showed well-defined crystal faces. The high-resolution TEM image demonstrated the crystallinity of the obtained material. The small size of the $CuFe_2O_4$ particles was beneficial for the fabrication of composites.

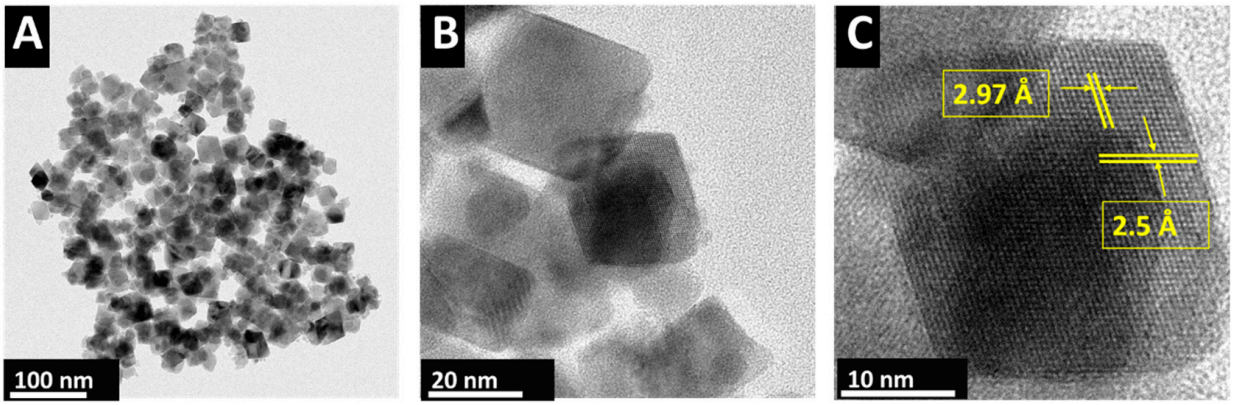


Figure 2. (**A**–**C**) TEM images of $CuFe_2O_4$ particles, prepared through hydrothermal synthesis. Spacings of 2.5 Å and 2.97 Å in the high-resolution image (**C**) correspond to d-spacings of crystallographic planes (211) and (112), respectively.

The composite materials were tested for applications in supercapacitor electrodes. Figure 3 compares the electrochemical testing results for the different composites, and the results are summarized in Table 1. It is obvious that the CV areas increased with the increasing PPy content in the composites (Figure 3A), which indicated a capacitance increase (Figure 3B). The CVs did not show redox peaks, which are typical for battery-type behavior [51,52]. The charge storage mechanism of $CuFe_2O_4$ is related to the reduction in Fe^{3+} and Cu^{2+} ions [40]. The charge and discharge times also increased with the increasing PPy content (Figure 3C) due to the capacitance increase. The electrodes showed good capacitance retention with the increasing sweep rate and current density (Figure 3 and Table 1). CFO50 and CFO30 showed C_S values at 1 mV s^{-1} of 3.60 and 4.52 F cm^{-2}, respectively, which were the highest capacitances of the composites studied in this investigation. The Cs values at 3 mA cm^{-2} of 3.90 and 4.60 F cm^{-2} were achieved for CFO50 and CFO30, respectively. As pointed out above, the fabrication of electrodes with the same thickness and same active mass loading presented difficulties for higher PPy content due to the lower density of PPy compared with the density of $CuFe_2O_4$.

Table 1. Capacitances of different composite electrodes.

Electrode	Capacitance from CV Data				Capacitance from GCD Data			
	1 mV s^{-1}		100 mV s^{-1}		3 mA cm^{-2}		40 mA cm^{-2}	
	C_S F cm^{-2}	C_m F g^{-1}	C_S F cm^{-2}	C_m F g^{-1}	C_S F cm^{-2}	C_m F g^{-1}	C_S F cm^{-2}	C_m F g^{-1}
CFO 100	1.2	31	0.85	21.7	1.17	29.9	0.63	16.14
CFO 90	1.5	39.2	1.1	29.35	1.46	38.5	1.22	32
CFO 70	2.53	63.8	2.07	52.2	2.6	66.7	2.22	55.84
CFO 50	3.6	91.1	1.87	47.1	3.9	113	2.7	68
CFO 30	4.52	117.37	2.24	58.4	4.6	120.1	3.56	92.68

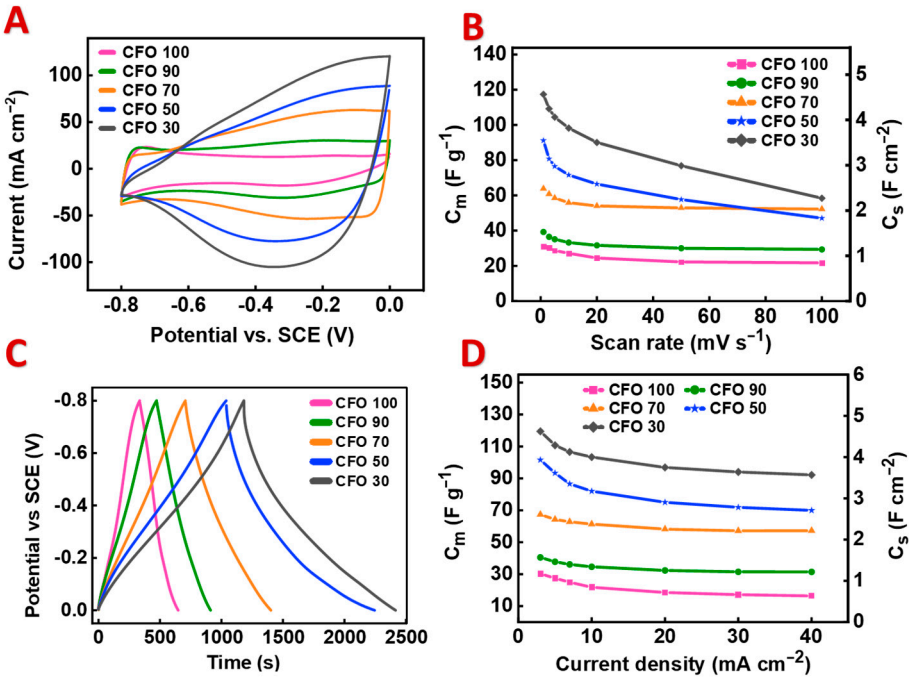


Figure 3. (**A**) CV data at 20 mV s^{-1}, (**B**) capacitances at different scan rates, (**C**) GCD data at 3 mA cm^{-2}, and (**D**) capacitances at different current densities for different composites.

Figure 4 shows the EIS data for the different composites. The Nyquist plot (Figure 4A) shows the impedance measurement data together with the simulation results obtained using the equivalent circuit presented in Figure 4B. The impedance decreased with the increasing PPy content. The real part of the impedance decreased due to the increased conductivity. The reduction in the imaginary part resulted from the increased capacitance. The equivalent circuit used for the simulation was developed for high-active-mass loading bulk electrodes [53]. It is known that porous electrodes can be described by transmission lines containing several RC elements [54–57]. The circuit presented in Figure 4B contains two RC(RQ) elements, where R, C, and Q represent the resistances, capacitance, and capacitive constant phase element, respectively. R_E, R_{CT}, and C_{DL} represent the electrolyte resistance, charge transfer resistance, and double-layer capacitance, respectively. The C′ increased with increasing PPy content in the composites. The relaxation frequency, given by the frequency of the C″ maximum, was relatively high; however, it decreased with increasing PPy content in the composites. The high capacitance retention observed in the CV and GCD data correlated with the relatively high EIS relaxation frequencies.

The analysis of the EIS data showed a significant reduction in the charge transfer resistance with the increasing PPy content in the range of 0–20% (Figure 5). As a result, at higher PPy contents, a significant capacitance increase was observed with increasing PPy concentration (Figure 5). This can result from the enhanced charge transfer at the interface of $CuFe_2O_4$ and PPy and the high capacitance of PPy. Moreover, PPy created an additional conductive percolating network in the composites. One of the problems limiting PPy applications in supercapacitor devices containing neutral electrolytes is poor cyclic stability [58]. A significant reduction in capacitance was reported during the first 1000 cycles in other composites containing magnetic particles and PPy [24]. This resulted from the poor cyclic stability of PPy. However, the investigation of the composites with high PPy contents revealed their good cyclic stability. Figure 6 shows the cycling stability test results for CFO50 and CFO30. The capacitance increased slightly at the beginning of cycling and remained nearly constant. The capacitance retention was 104.9% and 104.3% for CFO50 and CFO30, respectively, after 2000 cycles. The slight initial increase in the capacitance could be attributed to the microstructural changes within the electrode bulk.

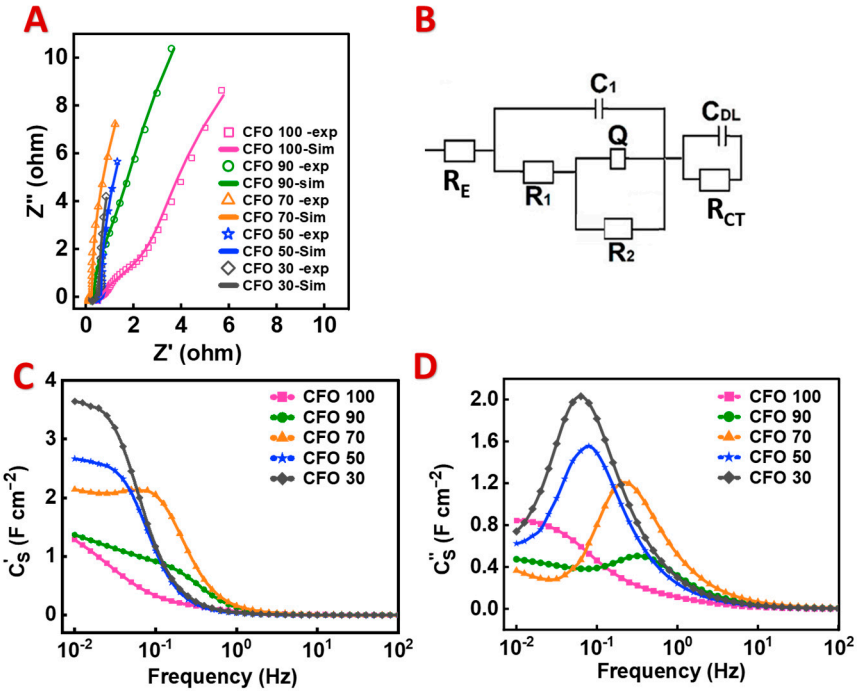


Figure 4. (**A**) Nyquist plots, (**B**) equivalent circuit model of EIS data, and (**C**,**D**) components of AC capacitance versus frequency.

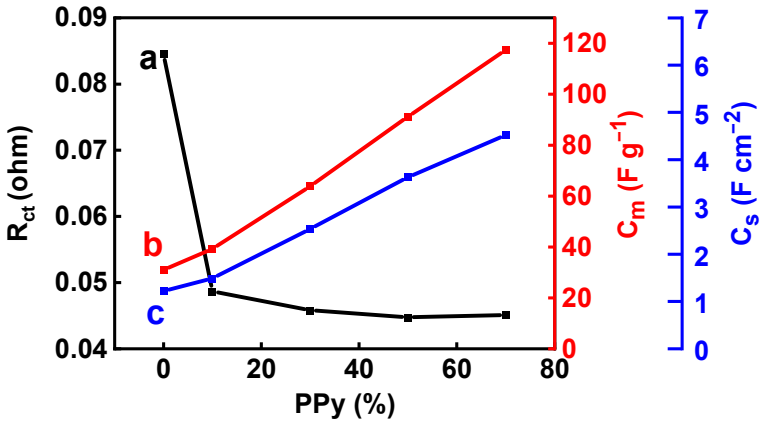


Figure 5. (a) R_{CT}, (b) C_m, and (c) C_S versus PPy content in the $CuFe_2O_4$ − PPy mixture.

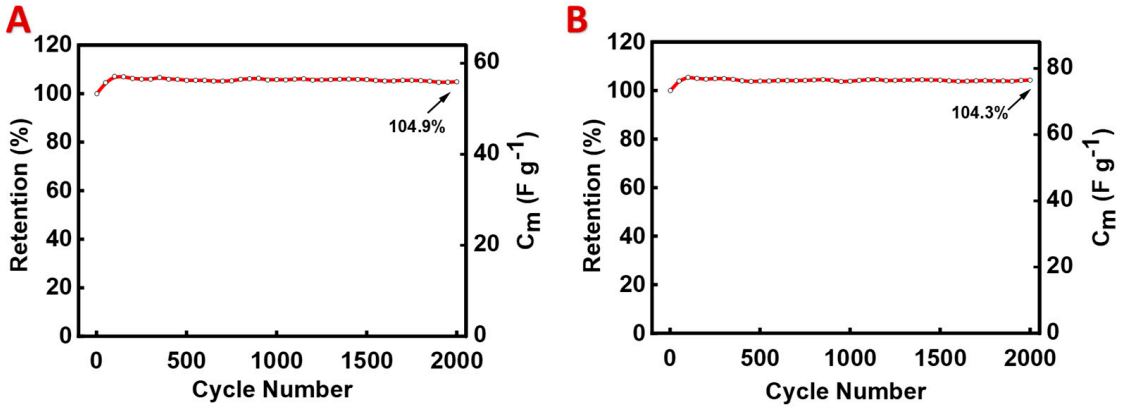


Figure 6. Cyclic stability data at a sweep rate of 50 mV s^{-1} for (**A**) CFO50 and (**B**) CFO30.

Figure 7 presents SEM images of the surface microstructures of the CFO50 and CFO30 composite electrodes, which showed the highest capacitances. The electrodes showed porous microstructures, which was beneficial for the electrolyte's diffusion. The typical pore size was <1 µm. The electrode porosity resulted from the packing of $CuFe_2O_4$, PPy, and MWCNT.

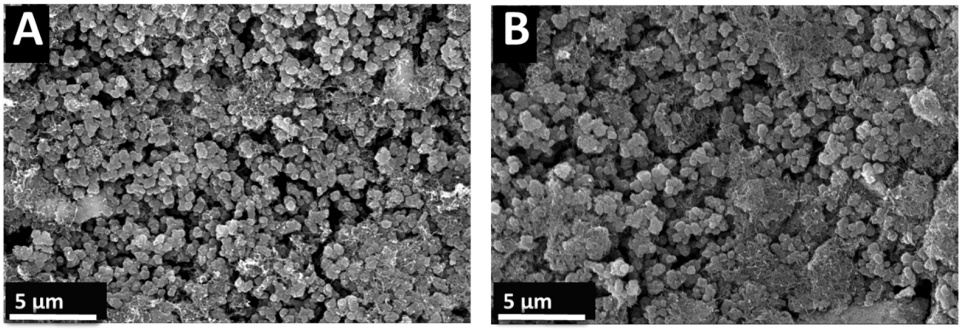


Figure 7. SEM images of surface microstructures of (**A**) CFO50 and (**B**) CFO30.

The relatively high capacitance of CFO50 and CFO30 is promising for energy storage in supercapacitors. Such composites showed higher capacitances compared with the composites containing other spinel and hexagonal ferrite ferrimagnetic ceramics with the same mass loading in the same potential range [24,25]. Moreover, CFO50 and CFO30 showed relatively high magnetization. Figure 8 shows the M–H curves plotted from the vibration magnetometer data. The CFO50 and CFO30 composites showed saturation magnetization values of 17.5 and 7.6 emu g^{-1}, respectively. Those values were lower than the CFO100 magnetization of 31.5 emu g^{-1} due to the lower $CuFe_2O_4$ content in the electrode. The coercivity values (H_c) from the hysteresis curves indicate that the CFO50 and CFO30 samples showed soft ferrimagnetic behavior, with H_c values between 50 and 100 Oe and a small remanent magnetization. This can result from the interaction of $CuFe_2O_4$ with the paramagnetic PPy [59,60]. The results of this study show that the properties of $CuFe_2O_4$ composites can be varied. Such composites belong to the category of magnetic pseudocapacitors [44], which are promising for various applications based on magnetoelectric and magnetocapacitive effects. The observation of capacitive properties in high-active-mass composites depends on using advanced Ni foam current collectors, which offer high corrosion resistance, conductivity, and porosity. However, the investigation of magnetocapacitive effects in electrodes prepared in this investigation presented difficulties since Ni is ferromagnetic, which generates its own magnetic field in an external magnetic field. Thus, non-magnetic current collectors with similar properties are needed. It should be noted that the composite $CuFe_2O_4$ spinel–PPy materials prepared in this investigation showed higher capacitances compared with other polymer composites containing various ferrimagnetic spinel compounds [40,61–63].

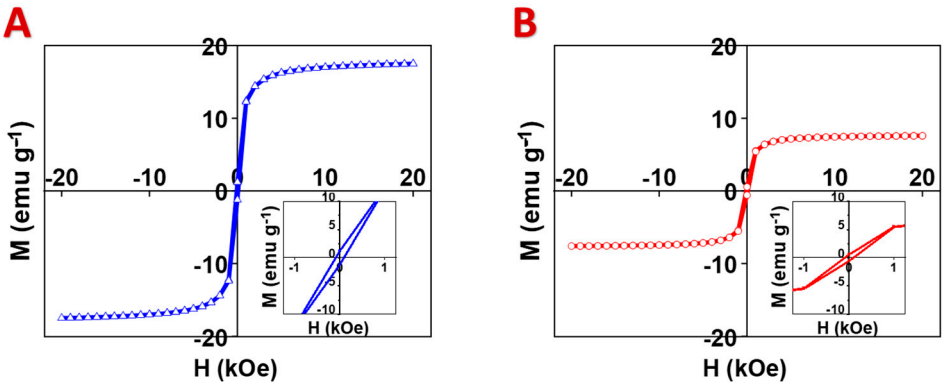


Figure 8. M–H curves for (**A**) CFO50 and (**B**) CFO30 (insets show low-field range).

4. Conclusions

Spinel $CuFe_2O_4$ nanoparticles with a crystal size of 20–30 nm and saturation magnetization of 31.4 emu g^{-1} were prepared by hydrothermal synthesis and used for the fabrication of $CuFe_2O_4$-PPy composites. The maximum PPy content in the composite electrodes of the same mass and thickness was 70%. The addition of PPy to $CuFe_2O_4$ reduced the charge transfer resistance and improved the material utilization at a high-active-mass loading of 40 mg cm^{-2}, enabling electrode fabrication with high C_S and C_m values. The capacitance increased with the increasing PPy content in the composites. The CFO50 and CFO30 composites showed the highest capacitances, which were 3.60 and 4.52 F cm^{-2} at 1 mVs^{-1} or 3.90 and 4.60 at 3 mA cm^{-2}, respectively. The obtained capacitances were higher compared with the capacitances of other composites of magnetic ceramic particles and PPy. The capacitance and magnetic properties of the composites can be varied. The magnetic behavior of the composites is influenced not only by the ferrimagnetic $CuFe_2O_4$ but also by the paramagnetic PPy. The composites belong to the category of magnetic supercapacitor materials and can potentially be used for energy storage and applications based on their magnetoelectric and magnetocapacitive properties. The use of ferromagnetic Ni for the fabrication of current collectors generates difficulties in the investigation of such properties. Future research must be focused on the replacement of commercial Ni foam current collectors with non-magnetic conductive current collectors for the investigation of magnetocapacitive and magnetoelectric effects. It is also expected that the development of new composites of conductive redox-active polymers with other magnetic materials and their solid solutions can result in advanced electrodes for energy storage and the capacitive deionization of water.

Author Contributions: Conceptualization, M.A. and I.Z.; methodology, M.A.; software, M.A.; validation, M.A.; formal analysis, M.A.; investigation, M.A.; resources, I.Z.; data curation, M.A.; writing—original draft preparation, M.A.; writing—review and editing, M.A. and I.Z.; visualization, M.A.; supervision, I.Z.; project administration, I.Z.; funding acquisition, I.Z. All authors have read and agreed to the published version of the manuscript.

Funding: This research was funded by the Natural Sciences and Engineering Research Council of Canada (grant RGPIN-2024-03968) and the CRC program.

Institutional Review Board Statement: Not applicable.

Informed Consent Statement: Not applicable.

Data Availability Statement: The data are available upon request.

Acknowledgments: The electron microscopy studies were performed at the Canadian Centre for Electron Microscopy.

Conflicts of Interest: The authors declare no conflicts of interest.

References

1. Romero, M.; Faccio, R.; Montenegro, B.; Tumelero, M.A.; Cid, C.C.P.; Pasa, A.A.; Mombrú, A.W. Role of conducting polyaniline interphase on the low field magnetoresistance for LSMO-PANI nanocomposites. *J. Magn. Magn. Mater.* **2018**, *466*, 446–451. [CrossRef]
2. Romero, M.; Faccio, R.; Pardo, H.; Tumelero, M.A.; Cid, C.C.P.; Pasa, A.A.; Mombrú, Á.W. Microstructure, interparticle interactions and magnetotransport of manganite-polyaniline nanocomposites. *Mater. Chem. Phys.* **2016**, *171*, 178–184. [CrossRef]
3. Pana, O.; Soran, M.; Leostean, C.; Macavei, S.; Gautron, E.; Teodorescu, C.; Gheorghe, N.; Chauvet, O. Interface charge transfer in polypyrrole coated perovskite manganite magnetic nanoparticles. *J. Appl. Phys.* **2012**, *111*, 044309. [CrossRef]
4. Vinayak, V.V.; Deshmukh, K.; Murthy, V.; Pasha, S.K. Conducting polymer based nanocomposites for supercapacitor applications: A review of recent advances, challenges and future prospects. *J. Energy Storage* **2024**, *100*, 113551. [CrossRef]
5. Snook, G.A.; Kao, P.; Best, A.S. Conducting-polymer-based supercapacitor devices and electrodes. *J. Power Sources* **2011**, *196*, 1–12. [CrossRef]
6. Dhandapani, E.; Thangarasu, S.; Ramesh, S.; Ramesh, K.; Vasudevan, R.; Duraisamy, N. Recent development and prospective of carbonaceous material, conducting polymer and their composite electrode materials for supercapacitor—A review. *J. Energy Storage* **2022**, *52*, 104937. [CrossRef]

7. Meng, Q.; Cai, K.; Chen, Y.; Chen, L. Research progress on conducting polymer based supercapacitor electrode materials. *Nano Energy* **2017**, *36*, 268–285. [CrossRef]
8. Tadesse, M.G.; Ahmmed, A.S.; Lübben, J.F. Review on conductive polymer composites for supercapacitor applications. *J. Compos. Sci.* **2024**, *8*, 53. [CrossRef]
9. Mahimai, B.M.; Li, E.; Pang, J.; Zhang, J.; Zhang, J. Interface engineering in conducting polymers-based supercapacitor. *J. Energy Storage* **2024**, *96*, 112598. [CrossRef]
10. Wustoni, S.; Ohayon, D.; Hermawan, A.; Nuruddin, A.; Inal, S.; Indartono, Y.S.; Yuliarto, B. Material design and characterization of conducting polymer-based supercapacitors. *Polym. Rev.* **2024**, *64*, 192–250. [CrossRef]
11. Gupta, K.; Jana, P.; Meikap, A.; Nath, T. Synthesis of $La_{0.67}Sr_{0.33}MnO_3$ and polyaniline nanocomposite with its electrical and magneto-transport properties. *J. Appl. Phys.* **2010**, *107*, 073704. [CrossRef]
12. Turcu, R.; Pana, O.; Nan, A.; Craciunescu, I.; Chauvet, O.; Payen, C. Polypyrrole coated magnetite nanoparticles from water based nanofluids. *J. Phys. D Appl. Phys.* **2008**, *41*, 245002. [CrossRef]
13. Amarnath, C.A.; Ghamouss, F.; Schmaltz, B.; Autret-Lambert, C.; Roger, S.; Gervais, F.; Tran-Van, F. Polypyrrole/lanthanum strontium manganite oxide nanocomposites: Elaboration and characterization. *Synth. Met.* **2013**, *167*, 18–24. [CrossRef]
14. Ren, X.; Wang, J.; Yin, H.; Tang, Y.; Fan, H.; Yuan, H.; Cui, S.; Huang, L. Hierarchical CoFe2O4@ PPy hollow nanocubes with enhanced microwave absorption. *Appl. Surf. Sci.* **2022**, *575*, 151752. [CrossRef]
15. Kateb, M.; Safarian, S.; Kolahdouz, M.; Fathipour, M.; Ahamdi, V. ZnO–PEDOT core–shell nanowires: An ultrafast, high contrast and transparent electrochromic display. *Sol. Energy Mater. Sol. Cells* **2016**, *145*, 200–205. [CrossRef]
16. Helli, M.; Sadrnezhaad, S.; Hosseini-Hosseinabad, S.; Vahdatkhah, P. Synthesis and characterization of CuO micro-flowers/PPy nanowires nanocomposites as high-capacity anode material for lithium-ion batteries. *J. Appl. Electrochem.* **2023**, *54*, 1–11. [CrossRef]
17. Yin, Z.; Ding, Y.; Zheng, Q.; Guan, L. CuO/polypyrrole core–shell nanocomposites as anode materials for lithium-ion batteries. *Electrochem. Commun.* **2012**, *20*, 40–43. [CrossRef]
18. Zhou, Y.; Jin, X.; Ni, J.; Zhang, S.; Yang, J.; Liu, P.; Wang, Z.; Lei, J. Evaporation induced uniform polypyrrole coating on CuO arrays for free-standing high lithium storage anode. *J. Solid State Electrochem.* **2019**, *23*, 1829–1836. [CrossRef]
19. Yin, Z.; Fan, W.; Ding, Y.; Li, J.; Guan, L.; Zheng, Q. Shell structure control of PPy-modified CuO composite nanoleaves for lithium batteries with improved cyclic performance. *ACS Sustain. Chem. Eng.* **2015**, *3*, 507–517. [CrossRef]
20. Qian, T.; Zhou, J.; Xu, N.; Yang, T.; Shen, X.; Liu, X.; Wu, S.; Yan, C. On-chip supercapacitors with ultrahigh volumetric performance based on electrochemically co-deposited CuO/polypyrrole nanosheet arrays. *Nanotechnology* **2015**, *26*, 425402. [CrossRef]
21. Ates, M.; Serin, M.A.; Ekmen, I.; Ertas, Y.N. Supercapacitor behaviors of polyaniline/CuO, polypyrrole/CuO and PEDOT/CuO nanocomposites. *Polym. Bull.* **2015**, *72*, 2573–2589. [CrossRef]
22. Xu, J.; Wang, D.; Yuan, Y.; Wei, W.; Gu, S.; Liu, R.; Wang, X.; Liu, L.; Xu, W. Polypyrrole-coated cotton fabrics for flexible supercapacitor electrodes prepared using CuO nanoparticles as template. *Cellulose* **2015**, *22*, 1355–1363. [CrossRef]
23. Awad, M.; Nawwar, M.; Zhitomirsky, I. Synergy of Charge Storage Properties of CuO and Polypyrrole in Composite CuO-Polypyrrole Electrodes for Asymmetric Supercapacitor Devices. *ACS Appl. Energy Mater.* **2024**, *7*, 5572–5581. [CrossRef]
24. MacDonald, M.; Zhitomirsky, I. Pseudocapacitive and Magnetic Properties of $SrFe_{12}O_{19}$–Polypyrrole Composites. *J. Compos. Sci.* **2024**, *8*, 351. [CrossRef]
25. MacDonald, M.; Zhitomirsky, I. Capacitive Properties of Ferrimagnetic $NiFe_2O_4$-Conductive Polypyrrole Nanocomposites. *J. Compos. Sci.* **2024**, *8*, 51. [CrossRef]
26. Dmitriev, A.I. Numerical model of a local contact of a polymer nanocomposite and its experimental validation. *Facta Univ. Ser. Mech. Eng.* **2021**, *19*, 079–089. [CrossRef]
27. Wang, K.; Alaluf, D.; Rodrigues, G.; Preumont, A. Precision shape control of ultra-thin shells with strain actuators. *J. Appl. Comput. Mech.* **2020**.
28. Xia, Q.; Xia, T.; Wu, X. PPy decorated α-Fe_2O_3 nanosheets as flexible supercapacitor electrodes. *Rare Met.* **2022**, *41*, 1195–1201. [CrossRef]
29. Liu, L.; Hu, X.; Zeng, H.-Y.; Yi, M.-Y.; Shen, S.-G.; Xu, S.; Cao, X.; Du, J.-Z. Preparation of NiCoFe-hydroxide/polyaniline composite for enhanced-performance supercapacitors. *J. Mater. Sci. Technol.* **2019**, *35*, 1691–1699. [CrossRef]
30. Beknalkar, S.A.; Teli, A.M.; Shin, J.C. Current innovations and future prospects of metal oxide electrospun materials for supercapacitor technology: A review. *J. Mater. Sci. Technol.* **2023**, *166*, 208–233. [CrossRef]
31. Zhang, Z.P.; Rong, M.Z.; Zhang, M.Q. Self-healable functional polymers and polymer-based composites. *Prog. Polym. Sci.* **2023**, *144*, 101724. [CrossRef]
32. Yuan, R.; Yin, X.; Gu, S.; Chang, J.; Li, H. Flexible double-wall carbon foam/Cu-Co oxides based symmetric supercapacitor with ultrahigh energy density. *J. Mater. Sci. Technol.* **2023**, *160*, 109–117. [CrossRef]
33. Birajdar, D.; Devatwal, U.; Jadhav, K. X-ray, IR and bulk magnetic properties of $Cu_{1+x}Mn_xFe_{2-2x}O_4$ ferrite system. *J. Mater. Sci.* **2002**, *37*, 1443–1448. [CrossRef]
34. Marinca, T.F.; Chicinaş, I.; Isnard, O. Structural and magnetic properties of the copper ferrite obtained by reactive milling and heat treatment. *Ceram. Int.* **2013**, *39*, 4179–4186. [CrossRef]

35. Lu, J.; Zhou, B.; Zhang, X.; Zhao, X.; Liu, X.; Wu, S.; Yang, D.-P. Oyster shell-derived $CuFe_2O_4$-Hap nanocomposite for healthy houses: Bacterial and formaldehyde elimination. *Chem. Eng. J.* **2023**, *477*, 147054. [CrossRef]
36. Ma, J.; Guo, X.; Ji, X. Amino-functionalized $CuFe_2O_4$ supported Pd nanoparticles as magnetically catalyst for H_2 production from methanolysis of ammonia borane and hydrogenation of nitro aromatics. *Int. J. Hydrogen Energy* **2024**, *51*, 345–356. [CrossRef]
37. Chen, Q.; Zhang, Y.; Xia, H.; Liu, R.; Wang, H. Fabrication of two novel amino-functionalized and starch-coated $CuFe_2O_4$-modified magnetic biochar composites and their application in removing Pb^{2+} and Cd^{2+} from wastewater. *Int. J. Biol. Macromol.* **2024**, *258*, 128973. [CrossRef]
38. Mostafa, E.M.; Hammam, R.E. Tailored solar collector coatings: Synthesis and characterization of $CuFe_2O_4$/PANI nanocomposites. *Opt. Mater.* **2024**, *156*, 115879. [CrossRef]
39. Guo, Y.; Chen, Y.; Hu, X.; Yao, Y.; Li, Z. Tween modified $CuFe_2O_4$ nanoparticles with enhanced supercapacitor performance. *Colloids Surf. A Physicochem. Eng. Asp.* **2021**, *631*, 127676. [CrossRef]
40. Liang, W.; Yang, W.; Sakib, S.; Zhitomirsky, I. Magnetic $CuFe_2O_4$ nanoparticles with pseudocapacitive properties for electrical energy storage. *Molecules* **2022**, *27*, 5313. [CrossRef]
41. Rushmittha, J.; Radhika, S.; Alrashidi, K.A.; Maheshwaran, G.; Dhinesh, S.; Sambasivam, S. Hybridization of $CuFe_2O_4$ by carbon microspheres with improved charge storage characteristics for high energy density solid-state hybrid supercapacitor. *Mater. Today Sustain.* **2024**, *28*, 100950. [CrossRef]
42. Nikam, P.N.; Patil, S.S.; Chougale, U.M.; Bajantri, T.H.; Fulari, A.V.; Fulari, V.J. Synthesis and characterization of $CuFe_2O_4$ spinel ferrite for supercapacitor application. *J. Indian Chem. Soc.* **2024**, *101*, 101277. [CrossRef]
43. Mbebou, M.; Polat, S.; Zengin, H. Sustainable cauliflower-patterned $CuFe_2O_4$ electrode production from chalcopyrite for supercapacitor applications. *Nanomaterials* **2023**, *13*, 1105. [CrossRef]
44. Sikkema, R.; Zhitomirsky, I. Magnetic supercapacitors: Charge storage mechanisms, magnetocapacitance, and magnetoelectric phenomena. *Appl. Phys. Rev.* **2023**, *10*, 021307. [CrossRef]
45. Ata, M.; Liu, Y.; Zhitomirsky, I. A review of new methods of surface chemical modification, dispersion and electrophoretic deposition of metal oxide particles. *Rsc Adv.* **2014**, *4*, 22716–22732. [CrossRef]
46. Conway, B.E. *Electrochemical Supercapacitors: Scientific Fundamentals and Technological Applications*; Springer Science & Business Media: Berlin/Heidelberg, Germany, 2013.
47. Taberna, P.; Simon, P.; Fauvarque, J.-F. Electrochemical characteristics and impedance spectroscopy studies of carbon-carbon supercapacitors. *J. Electrochem. Soc.* **2003**, *150*, A292. [CrossRef]
48. Al Kiey, S.A.; Ramadan, R.; El-Masry, M.M. Synthesis and characterization of mixed ternary transition metal ferrite nanoparticles comprising cobalt, copper and binary cobalt–copper for high-performance supercapacitor applications. *Appl. Phys. A* **2022**, *128*, 473. [CrossRef]
49. Khairy, M.; Bayoumy, W.; Selima, S.; Mousa, M. Studies on characterization, magnetic and electrochemical properties of nano-size pure and mixed ternary transition metal ferrites prepared by the auto-combustion method. *J. Mater. Res.* **2020**, *35*, 2652–2663. [CrossRef]
50. Berkowitz, A.; Schuele, W.; Flanders, P. Influence of crystallite size on the magnetic properties of acicular γ-Fe_2O_3 particles. *J. Appl. Phys.* **1968**, *39*, 1261–1263. [CrossRef]
51. Zan, G.; Li, S.; Chen, P.; Dong, K.; Wu, Q.; Wu, T. Mesoporous Cubic Nanocages Assembled by Coupled Monolayers with 100% Theoretical Capacity and Robust Cycling. *ACS Cent. Sci.* **2024**, *10*, 1283–1294. [CrossRef]
52. Li, J.; Dong, Z.; Chen, R.; Wu, Q.; Zan, G. Advanced nickel-based composite materials for supercapacitor electrodes. *Ionics* **2024**, *30*, 1833–1855. [CrossRef]
53. Wang, Y.; Liu, Y.; Zhitomirsky, I. Surface modification of MnO_2 and carbon nanotubes using organic dyes for nanotechnology of electrochemical supercapacitors. *J. Mater. Chem. A* **2013**, *1*, 12519–12526. [CrossRef]
54. Conway, B.; Pell, W. Power limitations of supercapacitor operation associated with resistance and capacitance distribution in porous electrode devices. *J. Power Sources* **2002**, *105*, 169–181. [CrossRef]
55. Conway, B.E.; Birss, V.; Wojtowicz, J. The role and utilization of pseudocapacitance for energy storage by supercapacitors. *J. Power Sources* **1997**, *66*, 1–14. [CrossRef]
56. Pell, W.; Conway, B.; Marincic, N. Analysis of non-uniform charge/discharge and rate effects in porous carbon capacitors containing sub-optimal electrolyte concentrations. *J. Electroanal. Chem.* **2000**, *491*, 9–21. [CrossRef]
57. Pell, W.G.; Conway, B.E. Voltammetry at a de Levie brush electrode as a model for electrochemical supercapacitor behaviour. *J. Electroanal. Chem.* **2001**, *500*, 121–133. [CrossRef]
58. Wu, C.; Wang, J.; Bai, Y.; Li, X. Significant effect of cations on polypyrrole cycle stability. *Solid State Ion.* **2020**, *346*, 115216. [CrossRef]
59. Aman, S.; Gouadria, S.; Ahmad, N.; Khan, S.A.; Manzoor, S.; Farid, H.M.T. The structural, dielectric and magnetic study of cobalt based spinel ferrites and polypyrrole composites. *J. Mater. Sci. Mater. Electron.* **2022**, *33*, 19534–19543. [CrossRef]
60. Bartl, A.; Dunsch, L.; Schmeißer, D.; Göpel, W.; Naarmann, H. Influence of oxygen on the paramagnetic properties of polypyrrole layers. *Synth. Met.* **1995**, *69*, 389–390. [CrossRef]
61. Ghasemi, A.K.; Ghorbani, M.; Lashkenari, M.S.; Nasiri, N. Facile synthesize of PANI/GO/$CuFe_2O_4$ nanocomposite material with synergistic effect for superb performance supercapacitor. *Electrochim. Acta* **2023**, *439*, 141685. [CrossRef]

62. Ishaq, S.; Moussa, M.; Kanwal, F.; Ayub, R.; Van, T.N.; Azhar, U.; Losic, D. One step strategy for reduced graphene oxide/cobalt-iron oxide/polypyrrole nanocomposite preparation for high performance supercapacitor electrodes. *Electrochim. Acta* **2022**, *427*, 140883. [CrossRef]
63. Senthilkumar, B.; Sankar, K.V.; Sanjeeviraja, C.; Selvan, R.K. Synthesis and physico-chemical property evaluation of PANI–$NiFe_2O_4$ nanocomposite as electrodes for supercapacitors. *J. Alloys Compd.* **2013**, *553*, 350–357. [CrossRef]

Disclaimer/Publisher's Note: The statements, opinions and data contained in all publications are solely those of the individual author(s) and contributor(s) and not of MDPI and/or the editor(s). MDPI and/or the editor(s) disclaim responsibility for any injury to people or property resulting from any ideas, methods, instructions or products referred to in the content.